To be published in Optics Letters:

Title:	Coupled Edge Modes Supported by a Microwave Metasurface
Authors:	Julia de Pineda,Alastair Hibbins,J. Sambles
Accepted:	30 January 20
Posted	03 February 20
DOI:	https://doi.org/10.1364/OL.384639

Coupled Edge modes supported by a Microwave Metasurface

J. D. DE PINEDA[1,*], A. P. HIBBINS[1], AND J. R. SAMBLES[1]

[1] Electromagnetic and Acoustic Materials Group, Department of Physics and Astronomy, University of Exeter, Stocker Road, Devon, EX4 4QL, United Kingdom
[*] jd602@exeter.ac.uk

Compiled February 1, 2020

Microwave metasurfaces comprised of overlapping layers of circular patches arranged in a hexagonal array are found to support edge modes akin to edge plasmons. The coupling of these edge modes across small gaps between two such arrays is explored. This phenomenon, well-known at optical frequencies is verified here for the first time at microwave frequencies.

http://dx.doi.org/10.1364/ao.XX.XXXXXX

1. INTRODUCTION

Localized electromagnetic surface waves can propagate at the interface between a conductor and an insulator. At visible frequencies they are known as surface plasmons and have widely been studied since the 1950s, e.g., [1]. At microwave frequencies, metals are often treated as perfect conductors, and as such are unable to support bound surface modes as the electromagnetic fields are completely excluded. However, when a surface pattern on a scale-length similar or smaller than the excitation wavelength is introduced, a mode similar in dispersion to a surface plasmon is found. This concept has been known since the mid-twentieth century [2, 3], and was readdressed theoretically and experimentally [4, 5] more recently. Pendry et. al. [4] showed that the dispersion of the modes supported on perfect conductors perforated with an array of subwavelength holes is governed by a surface boundary condition via an effective permittivity that is similar to that of Drude-like metals that support surface plasmons. This surface-plasmon-like behaviour can be extended to a wide range of surface textures. Since the size and spacing of the texturing elements can be controlled on all relevant length scales then it allows the creation of designer surface waves. Such textured structures that support the propagation of surface modes are known as metasurfaces. As their 3D analogues, metamaterials, metasurfaces can present material properties that are engineerable at the point of design, and can go beyond those presented by materials that are readily available in nature [6–8]. These types of structure are not exclusive to the microwave range but have also been explored in other areas of physics such as acoustics [9] and magnetism [10].

Metasurfaces represent a relatively easy way to manipulate the electromagnetic fields and have significant end-user interest. Some applications with particular commercial interest are the guiding of surface waves [11] and their transformation into different wave field configurations with desirable properties [12]. The electromagnetic properties of metasurfaces (i.e., surface impedance) and the shape of the modes supported can easily be controlled across the structure by simply varying the size or the shape of its elements [12], making them suitable for the manufacture of graded index devices such as lenses and leaky wave antennas [13–15]. In this work we focus on a metasurface that supports guided electromagnetic energy in a narrow dielectric region (surface waveguide) between two metasurface strips [16].

Edge states play an important role in condensed matter physics [17, 18] and lately they have found applications in many areas, including microwave engineering [19, 20]. Metasurfaces that support the propagation of edge modes have been studied for different applications, such as guiding energy on surfaces, steering them around sharp bends and splitting and redirecting energy between channels [21–23].

2. DESCRIPTION OF THE METASURFACE

The structure under study is a metasurface comprised of two layers, each layer being a hexagonal array of circular metal patches [16], arranged with respect to each other as a hexagonal close packed lattice. The unit cell of this structure is presented in Fig.1 (left). The top layer (blue) has been displaced by $\frac{p}{\sqrt{3}}$ in the x-direction with respect to the bottom layer (grey), where $p = 2.4\,\text{mm}$ is the lattice spacing of the structure. The circular metallic patches are made of copper, have a diameter $d = 2.15\,\text{mm}$ and are printed over a dielectric slab (PTE) of permittivity $\varepsilon = 2.8$ with a thickness of $t = 25\,\mu\text{m}$. The behaviour of this kind of layered structures is not simply determined by the resonances of its single elements but by the collective resonance of the constitutive elements and the overlap regions between them. These constitutive elements may be referred to as meta-molecules. The spacing between the layers should be made as small as possible to maximise the capacitive coupling between the layers and the confinement of the fields. However, this mainly only affects the dispersion of the surface modes which are strongly confined to the dielectric substrate [16].

Here we explore the interaction between two edge modes supported by lines of such meta-molecules, but we first examine the behavior of a single edge. A single hexagonal lattice geometry presents two sets of voids and therefore there are two available relative positions for the second layer with respect to

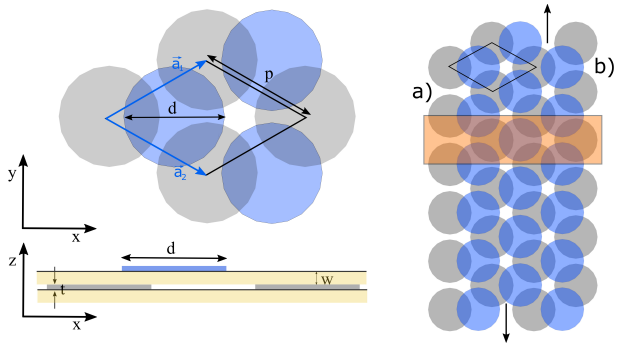

Fig. 1. (left) Unit cell (rhombic shape) of the structure comprised of two layers of copper patches printed over dielectric substrates. The bottom layer patches are coloured grey, and the upper layer are blue; the dielectric is represented in yellow. The diameter of the patches is $d = 2.15$ mm and the periodicity of the structure is $p = 2.4$ mm. The dielectric thickness is $w = 25\,\mu$m and the copper thickness is $t = 18\,\mu$m. The blue arrows represent the unit vectors of the structure in real space. (right) Sketch of the metasurface under study: The bottom layer is comprised of 4 rows of patches while the top layer has just three rows. The edge marked a) has just one overlap region and supports an edge mode while the edge marked b) has two overlap regions per edge patch and an edge mode is not supported.

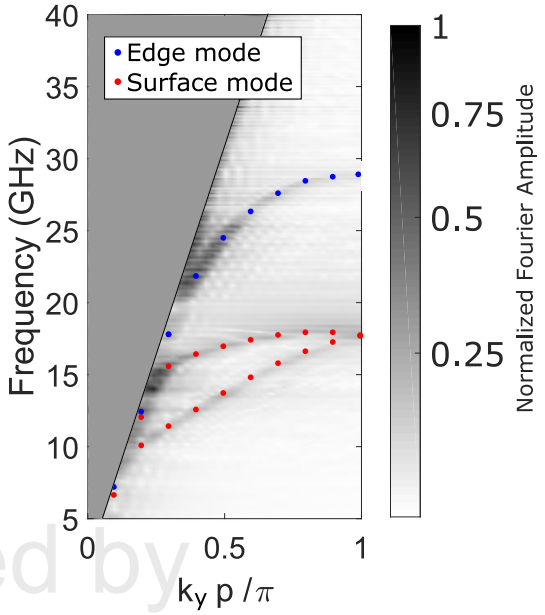

Fig. 2. Fourier amplitude spectra illustrating the dispersion of the modes supported by the single strip presented in Fig.1. The experimental dispersion is plotted as a gray scale and the FEM simulation data has been overlaid as dots. The structure supports the propagation of two surface modes (red) and one edge mode (blue).

the first. This results in two different possible edge terminations which support different modes. To support an edge mode, a structure needs to present free electric charges on its edge whilst ensuring that all patches have a zero net charge.

We have designed, built and characterized a strip which only supports the propagation of an edge mode along one of its edges for frequencies below 40 GHz. It is comprised of a bottom layer that is four patches wide and a top layer that is three patches wide. This strip is represented in Fig.1 (right).

One of the two edge-arrangements presents one overlap region per edge-patch (edge labelled a) in Fig. 1). Every metal patch must carry zero net charge, so the overlap region of the lower patch (grey) has a net electric charge of the same magnitude but opposite sign to the charge along the edge of the same patch. As there are then charges on the edge of the structure, an edge mode can propagate. The second termination b) in Fig.1 presents two overlap regions per edge-patch. This results in an edge mode at much higher frequency which was not observed in the experiments as being distinct from the light line.

The dispersion of the modes supported by the sample was modelled with a Finite Element Modelling (FEM) software [24] and measured experimentally. To obtain the experimental dispersion, two nominally identical loop-antennas are used, one of them as a source and the other one as a probe. They are each connected to a vector network analyser (VNA) via coaxial cables, and the frequency is swept between 5 GHz and 40 GHz. The source was placed at the mid-width of the strip while the probe is attached to an automated translation stage that scans along the long direction (y) of the strip on the opposite side of the sample. This configuration enables the recording of the amplitude and relative phase of the electromagnetic fields at every point in the frequency and spatial scan. A 1D Fast Fourier transform is then performed for every measured frequency, resulting in a frequency-wavevector dependence of the Fourier amplitude that illustrates the dispersion of the modes, shown in Fig.2. The experimental measurement is presented as a grey-scale plot and the modelled dispersion as dots. The FEM software calculates the eigenmodes supported by an infinite strip which resembles the experimental data when the length of the measured strip is long enough.

Two surface modes, each propagating in the y-direction along the 'bulk' of the metasurface (red), and one edge mode confined to the termination region (blue), are found. The number of supported surface modes is dictated by the number of meta-atoms in the transverse direction that comprise the structure [16].

3. COUPLING

The aim of this work is to study the interaction between a pair of the edge modes. For this purpose, two identical strips (parallel to the y-axis) have been fabricated, leaving a gap between them in the x-direction. The dispersion of the modes supported has been determined from experimental data and compared with simulation data from FEM software. Two different relative positions of the strips have been studied. In the first case, the edges are aligned to present mirror symmetry and in the second case we displace one by half of the period along the vertical direction to explore a glide symmetric configuration. For the glide symmetric case, as the patches are shifted in the vertical direction, the strips to be placed closer together.

Glide symmetry is a particular case of high symmetry, first introduced by Hessel et al. in 1973 [25]. For a structure to present glide symmetry it needs to be comprised of two lattices or sets of elements, one of which is the mirror image of the first one, that has been displaced by half the period of the lattice. Glide symmetry has the peculiarity that the band gap at the first Brillouin zone boundary for the two lowest order modes

is absent. As a consequence, the dispersion of the lowest order mode is straightened, resulting in a less frequency dependent behaviour [26, 27]. Glide-symmetric structures have widely been studied for both 1-dimensional systems [9, 28, 29] and 2-dimensional systems [30, 31].

A. Mirror-Symmetric configuration

A sample with mirror-symmetric edges was built and tested using the previously described VNA and translation stage setup. The source was placed in the gap between both strips and the probe was positioned on the opposite side of the sample, used to probe the electromagnetic field across a line in the center of the gap between the strips. A photograph of the sample is presented in Fig. 3. alongside the dispersion diagram (experimental and numerical) of the structure as well as the predicted normalised electric field distribution of the coupled edge modes at the Brillouin zone boundary.

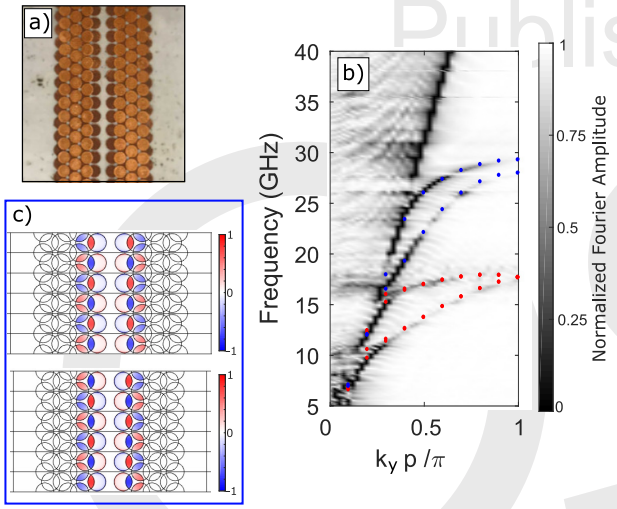

Fig. 3. a) Photograph of the sample used to study the coupling between two edge modes with a mirror-symmetric configuration of strips. Each strip is 3 patches wide on the top layer and 4 patches wide on the bottom layer. b) The grey-scale data is experimental data illustrating the dispersion of the modes supported. The modelled eigenmodes obtained with the FEM software have been overlaid as dots. Red dots represents the surface modes and blue dots the edge modes. c) Out-of-plane electric field distribution for the two coupled edge modes at the Brillouin zone boundary.
The higher energy one presents a symmetric field profile while the lower energy one has an anti-symmetric distribution.

In the dispersion diagram we find two families of modes. As in the first single-strip experiment, at lower frequencies (5 GHz to 20 GHz) we observe two surface modes. Each individual strip supports two surface modes as there are two full meta-molecules across the width of the structure. The two strips are identical to one another, and so the modes are degenerate. However, for small wave vectors, both the model and experiment predict a splitting. This is due to the interaction between equivalent modes in the neighbouring strips. This interaction is very weak as the fields of the surface modes are very confined to the dielectric spacing between the layers and only a very small fraction is available to interact with the other mode.

At higher frequencies we observe a second pair of modes that propagate along the inner edges of the structures. One of them propagates at a higher frequency than that expected for the edge mode of a single strip and a second one that propagates at a lower frequency. This splitting is due to the interaction and coupling between the modes. As the fields of the edge mode are less-well confined than the surface wave fields and extend to the surrounding space, the coupling between them is stronger. This coupling results in a pair of symmetric and anti-symmetric modes. The field plots of the higher energy symmetric mode and lower energy anti-symmetric mode are shown in Fig.3 b).

B. Glide-Symmetric Structure

Now we investigate the effect of glide symmetry on the interaction of the edge modes. To achieve this, one of the strips was displaced by half of the period in the y-direction. This symmetry transformation only significantly affects the coupling of the edge modes as it only changes the relative position of the two strips. Again, in the dispersion diagram of the structure, we find two families of modes. The surface modes, at lower frequencies, and the coupled edge modes, which propagate at higher frequencies. A photograph of the sample, the dispersion diagram of the modes supported, and the field plots for the edge modes are represented in Fig.4.

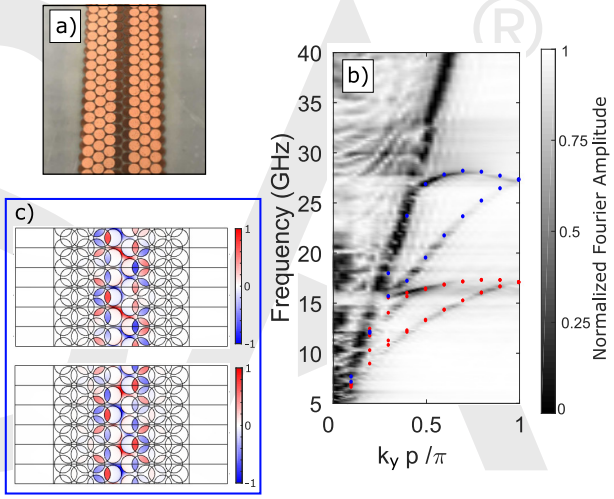

Fig. 4. a) Photograph of the sample used to study the coupling between two edge modes with a glide-symmetric configuration. Each strip is 3 patches wide on the top layer and 4 patches wide on the bottom layer. b) Experimental dispersion diagram of the glide-symmetric structure. The eigenmodes obtained with the FEM software have been overlaid as dots. The surface modes are represented by red dots and the edge modes by blue dots. c) Out-of-plane normalised electric field for the two coupled edge modes for $k_y p/\pi = 0.5$, where the distinction between the symmetric and anti-symmetric modes is clear.

The surface modes for this glide-symmetric structure remain at the same frequency as in the mirror-symmetric case. A small splitting in the surface modes is again observed. However, the edge modes show the effect of glide symmetry. The gap at the Brillouin zone boundary between the pair of coupled edge modes is closed and the lowest frequency mode has a more linear dispersion. As for the field distribution, a distinction between a symmetric high frequency mode and and an anti-symmetric mode at a lower frequency is observed (Fig. 4 b), represented at $k_y = 0.5\frac{\pi}{p}$). However, this is lost as we move

towards the Brillouin zone boundary where the two modes become degenerate.

C. Separation effect

Finally, we studied the effect that the separation between the strips has on the coupling of the edge modes. We have run simulations for three different distances between the strips for both configurations. For the case where the strips have mirror symmetry the band gap at the Brillouin zone edge between the coupled edge modes increases up to 5 GHz when the strips are only 0.2 mm away from each other. Meanwhile, for the glide-symmetric case, the coupling weakens as the strips are pulled apart from each other while the degeneracy at the Brillouin zone boundary is maintained.

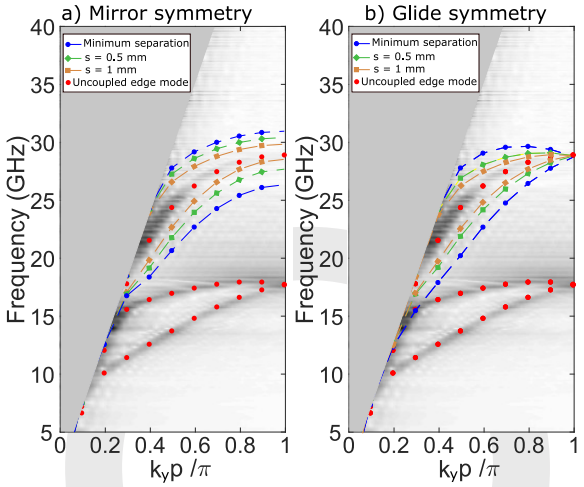

Fig. 5. Dispersion diagrams of the modes supported by the coupled-edge-mode structures for three different separations of the strips (1 mm, 0.5 mm and 0.2 mm). They have been plotted on top of the experimental data of a single strip (gray-scale). The mirror-symmetric case is represented on the left and the glide symmetry case on the right.

4. CONCLUSION

The coupling of microwave edge modes supported by a pair of metasurfaces has been quantified and the results compared with the predictions from a numerical model. We have also observed coupling between the surface waves supported but this is much weaker than the edge mode coupling because of the strong confinement of the electromagnetic fields. Further, the effect of glide symmetry on the pair of coupled edge modes has been investigated. The glide symmetry closes the gap between the coupled edge modes at the Brillouin zone boundary and hence yields a more linear dispersion of the lowest order mode. This study illustrates fully the potential for designer edge states with metasurfaces and thereby novel ways to manipulate microwaves energy and data.

Funding. We thank the EPSRC for their financial support. (Grant No. EP/L015331/1), CDT metamaterials. J.P.G. wishes to thank Flann Microwave Ltd (Bodmin, UK) for additional financial support.

Acknowledgement. All data created during this research are openly available from the University of Exeter's institutional repository at https://ore.exeter.ac.uk/repository/

Disclosures. The authors declare no conflicts of interest.

REFERENCES

1. R. H. Ritchie, Phys. Rev. **106**, 874 (1957).
2. C. C. Cutler, "Genesis of the corrugated electromagnetic surface," in *Proceedings of IEEE Antennas and Propagation Society International Symposium and URSI National Radio Science Meeting,* , vol. 3 (1994), pp. 1456–1459.
3. A. A. Oliner and A. Hessel, IRE Transactions on Antennas Propag. **7**, 201 (1959).
4. J. B. Pendry, L. Martín-Moreno, and F. J. Garcia-Vidal, Science. **305**, 847 (2004).
5. A. Hibbins, B. Evans, and J. Sambles, Science. **308**, 670 (2005).
6. S. B. Glybovski, S. A. Tretyakov, P. A. Belov, Y. S. Kivshar, and C. R. Simovski, Phys. Reports **634**, 1 (2016). Metasurfaces: From microwaves to visible.
7. H.-T. Chen, A. J. Taylor, and N. Yu, Reports on Prog. Phys. **79**, 076401 (2016).
8. J. D. de Pineda, G. P. Ward, A. P. Hibbins, and J. R. Sambles, Phys. Rev. B **100**, 081409 (2019).
9. J. G. Beadle, I. R. Hooper, J. R. Sambles, and A. P. Hibbins, The J. Acoust. Soc. Am. **145**, 3190 (2019).
10. R. Shindou, J.-i. Ohe, R. Matsumoto, S. Murakami, and E. Saitoh, Phys. Rev. B **87**, 174402 (2013).
11. J. B. Pendry, D. Schurig, and D. R. Smith, Science **312**, 1780 (2006).
12. S. Maci, G. Minatti, M. Casaletti, and M. Bosiljevac, IEEE Antennas Wirel. Propag. Lett. **10**, 1499 (2011).
13. J. A. Dockrey, M. J. Lockyear, S. J. Berry, S. A. R. Horsley, J. R. Sambles, and A. P. Hibbins, Phys. Rev. B **87**, 1 (2013).
14. J. D. de Pineda, R. C. Mitchell-Thomas, A. P. Hibbins, and J. R. Sambles, Appl. Phys. Lett. **111**, 211603 (2017).
15. G. Minatti, M. Faenzi, E. Martini, F. Caminita, P. De Vita, D. Gonzalez-Ovejero, M. Sabbadini, and S. Maci, IEEE Transactions on Antennas Propag. **63**, 1288 (2015).
16. J. D. de Pineda, A. P. Hibbins, and J. R. Sambles, Phys. Rev. B **98**, 205426 (2018).
17. L. Lu, J. D. Joannopoulos, and M. Soljačić, Nat. Photonics **8**, 821 (2014).
18. Z. Wang, Y. Chong, J. D. Joannopoulos, and M. Soljačić, Nature **461**, 772 (2009).
19. T. Ma, A. B. Khanikaev, S. H. Mousavi, and G. Shvets, Phys. Rev. Lett. **114**, 127401 (2015).
20. Z. Qiao, J. Jung, C. Lin, Y. Ren, A. H. MacDonald, and Q. Niu, Phys. Rev. Lett. **112**, 206601 (2014).
21. R. D. Meade, K. D. Brommer, A. M. Rappe, and J. D. Joannopoulos, Phys. Rev. B **44**, 10961 (1991).
22. A. B. Khanikaev, R. Fleury, S. H. Mousavi, and A. Alù, Nat. Commun. **6**, 8260 (2015).
23. A. B. Khanikaev and G. Shvets, Nat. Photonics **11**, 763 (2017).
24. COMSOL, Inc, "Comsol multiphysics," .
25. A. Hessel, A. A. Oliner, M. H. Chen, and R. C. Li, Proc. IEEE **61**, 183 (1973).
26. M. Ebrahimpouri, O. Quevedo-Teruel, and E. Rajo-Iglesias, IEEE Microw. Wirel. Components Lett. **27**, 542 (2017).
27. J. D. de Pineda, R. C. Mitchell-Thomas, A. P. Hibbins, and J. R. Sambles, "Hexagonal symmetry metasurfaces for broadband antenna applications," in *2017 IEEE International Symposium on Antennas and Propagation USNC/URSI National Radio Science Meeting,* (2017), pp. 831–832.
28. M. Camacho, R. C. Mitchell-Thomas, A. P. Hibbins, J. R. Sambles, and O. Quevedo-Teruel, Opt. Lett. **42**, 3375 (2017).
29. R. Quesada, D. Martín-Cano, F. J. García-Vidal, and J. Bravo-Abad, Opt. Lett. **39**, 2990 (2014).
30. E. Rajo-Iglesias, M. Ebrahimpouri, and O. Quevedo-Teruel, IEEE Microw. Wirel. Components Lett. **28**, 476 (2018).
31. O. Quevedo-teruel, M. Ebrahimpouri, and M. N. M. Kehn, IEEE Antennas Wirel. Propag. Lett. **15**, 484 (2016).

FULL REFERENCES

1. R. H. Ritchie, "Plasma losses by fast electrons in thin films," Phys. Rev. **106**, 874–881 (1957).
2. C. C. Cutler, "Genesis of the corrugated electromagnetic surface," in *Proceedings of IEEE Antennas and Propagation Society International Symposium and URSI National Radio Science Meeting,* vol. 3 (1994), pp. 1456–1459.
3. A. A. Oliner and A. Hessel, "Guided Waves on Sinusoidally-Modulated Reactance Surfaces," IRE Transactions on Antennas Propag. **7**, 201–208 (1959).
4. J. B. Pendry, L. Martín-Moreno, and F. J. Garcia-Vidal, "Mimicking surface plasmons with structured surfaces." Science. **305**, 847–8 (2004).
5. A. Hibbins, B. Evans, and J. Sambles, "Experimental verification of designer surface plasmons," Science. **308**, 670–672 (2005).
6. S. B. Glybovski, S. A. Tretyakov, P. A. Belov, Y. S. Kivshar, and C. R. Simovski, "Metasurfaces: From microwaves to visible," Phys. Reports **634**, 1 – 72 (2016). Metasurfaces: From microwaves to visible.
7. H.-T. Chen, A. J. Taylor, and N. Yu, "A review of metasurfaces: physics and applications," Reports on Prog. Phys. **79**, 076401 (2016).
8. J. D. de Pineda, G. P. Ward, A. P. Hibbins, and J. R. Sambles, "Metasurface bilayer for slow microwave surface waves," Phys. Rev. B **100**, 081409 (2019).
9. J. G. Beadle, I. R. Hooper, J. R. Sambles, and A. P. Hibbins, "Broadband, slow sound on a glide-symmetric meander-channel surface," The J. Acoust. Soc. Am. **145**, 3190–3194 (2019).
10. R. Shindou, J.-i. Ohe, R. Matsumoto, S. Murakami, and E. Saitoh, "Chiral spin-wave edge modes in dipolar magnetic thin films," Phys. Rev. B **87**, 174402 (2013).
11. J. B. Pendry, D. Schurig, and D. R. Smith, "Controlling Electromagnetic Fields," Science **312**, 1780–1782 (2006).
12. S. Maci, G. Minatti, M. Casaletti, and M. Bosiljevac, "Metasurfing : Addressing Waves on Impenetrable Metasurfaces," IEEE Antennas Wirel. Propag. Lett. **10**, 1499–1502 (2011).
13. J. A. Dockrey, M. J. Lockyear, S. J. Berry, S. A. R. Horsley, J. R. Sambles, and A. P. Hibbins, "Thin metamaterial Luneburg lens for surface waves," Phys. Rev. B **87**, 1–5 (2013).
14. J. D. de Pineda, R. C. Mitchell-Thomas, A. P. Hibbins, and J. R. Sambles, "A broadband metasurface luneburg lens for microwave surface waves," Appl. Phys. Lett. **111**, 211603 (2017).
15. G. Minatti, M. Faenzi, E. Martini, F. Caminita, P. De Vita, D. Gonzalez-Ovejero, M. Sabbadini, and S. Maci, "Modulated Metasurface Antennas for Space: Synthesis, Analysis and Realizations," IEEE Transactions on Antennas Propag. **63**, 1288–1300 (2015).
16. J. D. de Pineda, A. P. Hibbins, and J. R. Sambles, "Microwave edge modes on a metasurface with glide symmetry," Phys. Rev. B **98**, 205426 (2018).
17. L. Lu, J. D. Joannopoulos, and M. Soljačić, "Topological photonics," Nat. Photonics **8**, 821 (2014).
18. Z. Wang, Y. Chong, J. D. Joannopoulos, and M. Soljačić, "Observation of unidirectional backscattering-immune topological electromagnetic states," Nature **461**, 772–775 (2009).
19. T. Ma, A. B. Khanikaev, S. H. Mousavi, and G. Shvets, "Guiding electromagnetic waves around sharp corners: Topologically protected photonic transport in metawaveguides," Phys. Rev. Lett. **114**, 127401 (2015).
20. Z. Qiao, J. Jung, C. Lin, Y. Ren, A. H. MacDonald, and Q. Niu, "Current partition at topological channel intersections," Phys. Rev. Lett. **112**, 206601 (2014).
21. R. D. Meade, K. D. Brommer, A. M. Rappe, and J. D. Joannopoulos, "Electromagnetic bloch waves at the surface of a photonic crystal," Phys. Rev. B **44**, 10961–10964 (1991).
22. A. B. Khanikaev, R. Fleury, S. H. Mousavi, and A. Alù, "Topologically robust sound propagation in an angular-momentum-biased graphene-like resonator lattice," Nat. Commun. **6**, 8260 (2015).
23. A. B. Khanikaev and G. Shvets, "Two-dimensional topological photonics," Nat. Photonics **11**, 763–773 (2017).
24. COMSOL, Inc, "Comsol multiphysics," .
25. A. Hessel, A. A. Oliner, M. H. Chen, and R. C. Li, "Propagation in Periodically Loaded Waveguides with Higher Symmetries," Proc. IEEE **61**, 183–195 (1973).
26. M. Ebrahimpouri, O. Quevedo-Teruel, and E. Rajo-Iglesias, "Design Guidelines for Gap Waveguide Technology Based on Glide-Symmetric Holey Structures," IEEE Microw. Wirel. Components Lett. **27**, 542–544 (2017).
27. J. D. de Pineda, R. C. Mitchell-Thomas, A. P. Hibbins, and J. R. Sambles, "Hexagonal symmetry metasurfaces for broadband antenna applications," in *2017 IEEE International Symposium on Antennas and Propagation USNC/URSI National Radio Science Meeting,* (2017), pp. 831–832.
28. M. Camacho, R. C. Mitchell-Thomas, A. P. Hibbins, J. R. Sambles, and O. Quevedo-Teruel, "Designer surface plasmon dispersion on a one-dimensional periodic slot metasurface with glide symmetry," Opt. Lett. **42**, 3375–3378 (2017).
29. R. Quesada, D. Martín-Cano, F. J. García-Vidal, and J. Bravo-Abad, "Deep-subwavelength negative-index waveguiding enabled by coupled conformal surface plasmons," Opt. Lett. **39**, 2990–2993 (2014).
30. E. Rajo-Iglesias, M. Ebrahimpouri, and O. Quevedo-Teruel, "Wideband phase shifter in groove gap waveguide technology implemented with glide-symmetric holey ebg," IEEE Microw. Wirel. Components Lett. **28**, 476–478 (2018).
31. O. Quevedo-teruel, M. Ebrahimpouri, and M. N. M. Kehn, "Ultrawideband Metasurface Lenses Based on Off-Shifted Opposite Layers," IEEE Antennas Wirel. Propag. Lett. **15**, 484–487 (2016).